C Journal of
COMPUTATIONAL
CHEMISTRY

WWW.C-CHEM.ORG

FULL PAPER

Check for updates

Understanding the Role of Surface Oxygen in Hg Removal on Un-Doped and Mn/Fe-Doped CeO$_2$(111)

Ping Liu,[a] Lixia Ling,[b] Hao Lin,[b] and Baojun Wang [iD]*[c]

Effects of surface-adsorbed O and lattice O for the CeO$_2$(111) surface on Hg removal has been researched. In this work, periodic calculations based on density functional theory (DFT) were performed with the on-site Coulomb interaction. Hg is oxidized to HgO via the surface-adsorbed O by overcoming a Gibbs free energy barrier of 114.1 kJ·mol^{-1} on the CeO$_2$(111) surface. Mn and Fe doping reduce the activation Gibbs free energy for the Hg oxidation, and energies of 70.7 and 49.6 kJ·mol^{-1} are needed on Ce$_{0.96}$Mn$_{0.04}$O$_2$(111) and Ce$_{0.96}$Fe$_{0.04}$O$_2$(111) surfaces. Additionally, lattice O also plays an important role in Hg removal. Hg cannot be oxidized leading to the formation of

HgO on the un-doped CeO$_2$(111) surface owing to the inertness of lattice O, which can be easily oxidized to HgO on Ce$_{0.96}$Mn$_{0.04}$O$_2$(111) and Ce$_{0.96}$Fe$_{0.04}$O$_2$(111) surfaces. It can be seen that both surface-adsorbed O and lattice O play important roles in removing Hg. The present study will shed light on understanding and developing Hg removal technology on un-doped and Mn/Fe-doped CeO$_2$(111) catalysts. © 2019 Wiley Periodicals, Inc.

Introduction

CeO$_2$ is a typical rare earth metal oxide, Ce^{3+}/Ce^{4+} can be transformed into each other in ceria. Therefore, CeO$_2$ has a favorable ability to storage and release oxygen, as well as unique catalytic oxidation performance,[1,2] which has been widely used in catalytic field.[3,4] Hg is difficult to remove due to its reaction inertia, high volatility, toxicity[5–8] and also shows a detrimental effect on environment and human health.[9–11] Therefore, it has got a lot of attentions.

CeO$_2$ is an effective component for Hg removal.[12] CeO$_2$ had been loaded on the HZSM-5 to remove Hg in the exhaust gas, and the result showed that HgO was generated in flue gas via oxidizing Hg with surface active oxygen by TG analysis.[13] The same results could be obtained by loading CeO$_2$ on the activated carbon fiber,[14] activated coke,[15] and activated carbon.[16] In addition, Hg was oxidized to HgO on CuO-CeO$_2$/TiO$_2$ (CuCeTi)[17] and CeO$_2$/HZSM-5[13] catalysts, and HgO could be transformed into Hg under a selective catalytic reduction (SCR) atmosphere. It showed that ceria-based catalysts could be cyclic utilized to remove Hg.

Meanwhile, plenty of experimental and theoretical results showed that the introduction of the second metal could greatly improve the activity of surface O and oxidation capacity of CeO$_2$. CO adsorption on un-doped CeO$_2$(111) and Mn-doped CeO$_2$(111) surfaces had been studied by using the DFT method, and the results showed that there were three adsorption modes for CO on the Mn-doped CeO$_2$(111), including physical, chemical adsorption and the oxidation state CO$_2$ by CO binding with the surface O, but only physical adsorption on the un-doped CeO$_2$(111) surface.[18] In addition, the Mn-doped increased the activity of the lattice O and the O vacancy formation energy was 0.46 eV, which was far less than un-doped CeO$_2$(111) surface (2.08 eV).[19] It contributed to the easy oxidation of CO to

CO$_2$ on the Mn-doped CeO$_2$(111). Nie et al.[20] had also investigated the oxidation of CO on the Pt-doped CeO$_2$ surface and found that the doping of the Pt atom greatly increased the activity of lattice O on the CeO$_2$ surface, thus effectively accelerated the oxidation of CO. Additionally, NO$_2$ can be easily formed NO$_3^-$ on Mn- or Fe-doped CeO$_2$(111) surface, and adsorption energies of NO on different surfaces can be sorted according to the order of MnCe > FeCe > CeO$_2$.[21] Similarly, the doping of Mn on CeO$_2$ surface had been proved to have a good capacity for resisting the poisoning of SO$_2$[22] and removing heavy metal Hg,[23] and the performance of Hg removal was improved by doping MnO$_2$ on γ-Al$_2$O$_3$ supported ceria.[23]

The object of this work is to explore the effect of surface-adsorbed O and lattice O on ceria catalyst for eliminating Hg. The mechanism of oxidizing Hg has been investigated, and the activity for two types of O on un-doped, Mn-, and Fe-doped CeO$_2$(111) have been explored. And the roles of surface-

[a] P. Liu
State Key Laboratory of Coal Conversion, Institute of Coal Chemistry, Chinese Academy of Sciences, Taiyuan 030001, People's Republic of China
[b] L. Ling, H. Lin
College of Chemistry and Chemical Engineering, Taiyuan University of Technology, Taiyuan 030024, People's Republic of China
[c] B. Wang
Key Laboratory of Coal Science and Technology of Ministry of Education and Shanxi Province, Taiyuan University of Technology, Taiyuan 030024, People's Republic of China
E-mail: wangbaojun@tyut.edu.cn or wbj@tyut.edu.cn

Wiley Online Library

J. Comput. Chem. **2019**, *40*, 2611–2621 **2611**

adsorbed O and lattice O, as well as Mn and Fe dopant in removing Hg will be discussed and summarized.

Computational Details

Models

CeO$_2$(111) surface is stable and the most exposed surface of ceria.[24–26] The slab was constructed via a $p(3 \times 3)$ supercell with nine atomic layers[27] (including 27 Ce atom and 54 O atom) with a 15 Å vacuum thickness, as shown in Figure 1a and 1b. To simulate Mn- and Fe-doped CeO$_2$(111) surfaces, a Mn or Fe atom takes place of one Ce atom, which are Ce$_{0.96}$Mn$_{0.04}$O$_2$(111) and Ce$_{0.96}$Fe$_{0.04}$O$_2$(111), can be observed in Figure 1c and 1d.[28] Mn and Fe-doped CeO$_2$(111) with O vacancy models were also built by removing a O atom from Ce$_{0.96}$Mn$_{0.04}$O$_2$(111) and Ce$_{0.96}$Fe$_{0.04}$O$_2$(111) surfaces, and Ce$_{0.96}$Mn$_{0.04}$O$_{2-x}$(111) and Ce$_{0.96}$Fe$_{0.04}$O$_{2-x}$(111) surfaces are shown in Figure 1e and 1f. Except for the top six atomic layers and the adsorbates, other atoms were fixed.

Computational method

The first principle calculations were performed based on spin-polarized density functional theory (DFT) method using the Perdew–Burke–Ernzerhof (PBE) functional[29] as implemented in Vienna ab initio simulation package (VASP) code.[30,31] The core–valence interaction was described by the projector-augmented wave (PAW) method.[32,33] A plane wave energy cutoff of 400 eV and electronic occupancies were determined according to the Gaussian scheme with an energy smearing of 0.2 eV. The force on all the relaxed atoms was converged to 0.02 eV·Å^{-1} and the energy difference was lower than 10^{-5} eV when geometries were optimized. Calculations on ceria bulk with a k-point mesh of $6 \times 6 \times 6$ gave a result with better accuracy of 5.438 Å compared to the experimental value of 5.411 Å,[34] which was in good agreement with previous work.[35,36] The 3×3×1 Monkhorst–Pack grid for surface was used. In the whole calculation process, we considered the spin polarization effect on the system, spin polarized calculation
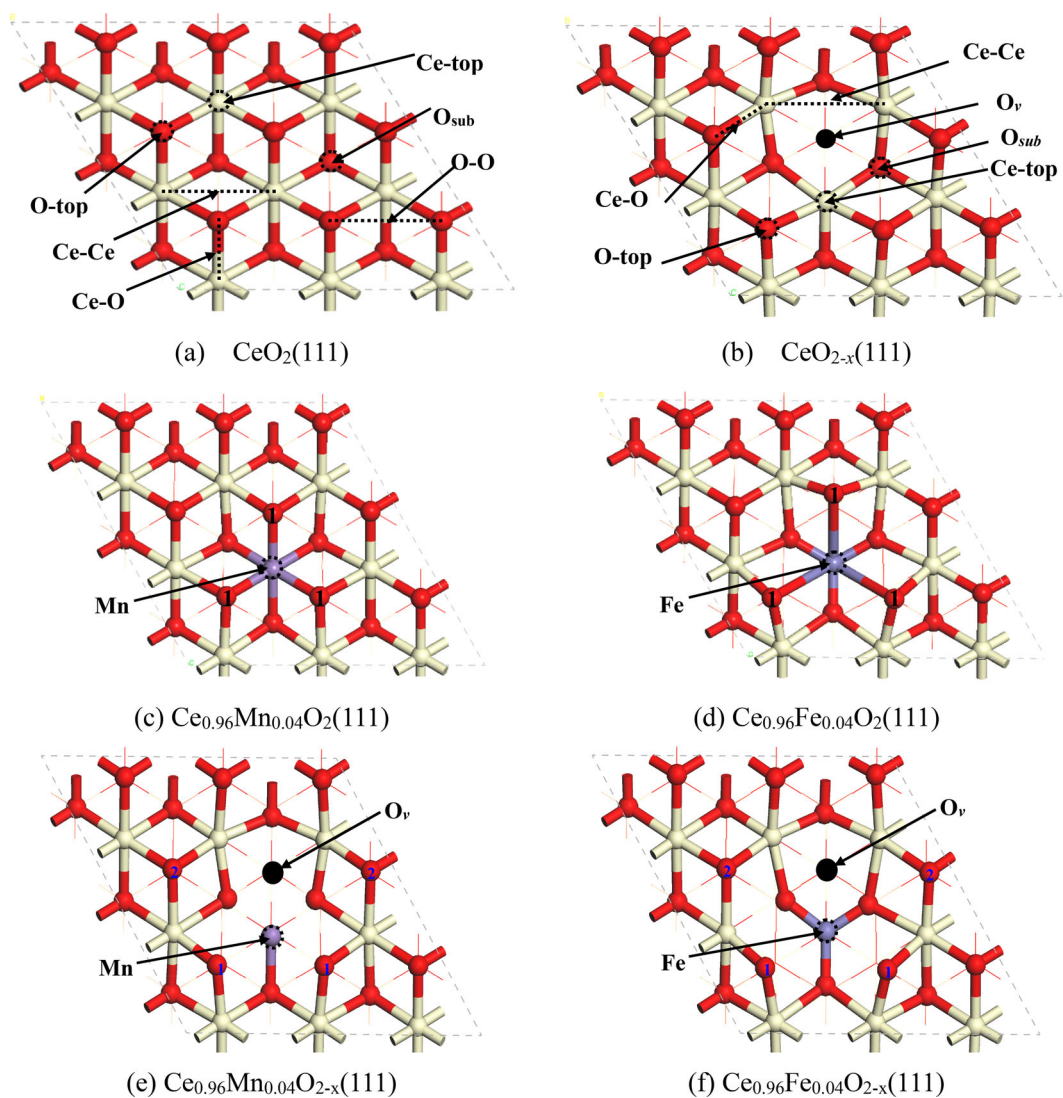
Figure 1. (a) CeO$_2$(111), (b) CeO$_{2-x}$(111), (c) Ce$_{0.96}$Mn$_{0.04}$O$_2$(111), (d) Ce$_{0.96}$Fe$_{0.04}$O$_2$(111), (e) Ce$_{0.96}$Mn$_{0.04}$O$_{2-x}$(111), and (f) Ce$_{0.96}$Fe$_{0.04}$O$_{2-x}$(111) surfaces. [Color figure can be viewed at wileyonlinelibrary.com]

was performed and the parameter of ISPIN was selected as 2 in the INCAR file. For the DFT + U calculations, U Hubbard values of 5.0 eV for Ce,[37,38] 4.5 eV for Mn,[39,40] and 4.3 eV for Fe[41,42] were applied.

In this work, adsorption ability of different species is estimated using adsorption energy (E_{ads}), which is defined as:

$$E_{ads} = E_{adsorbate + slab} - E_{slab} - E_{adsorbate} \qquad (1)$$

where $E_{adsorbate + slab}$ is the total energy of the interacting adsorbate-slab system, E_{slab} and $E_{adsorbate}$ are total energies of the un-doped or Mn/Fe-doped $CeO_2(111)$ surfaces and the molecule in the gas phase, respectively.

The climbing-image nudged elastic band (CI-NEB) method[43,44] combining with the dimmer method was used to determine the transition states (TSs) for the elementary reaction, in which the image close to the transition structure obtained by CI-NEB was further optimized by using the dimer method[45,46] and was confirmed by the existence of one imaginary frequency. In addition, Gibbs free energy profiles of Hg oxidation by surface-adsorbed O on regular $CeO_2(111)$ surface, as well as Hg cyclic oxidation on $Ce_{0.96}Mn_{0.04}O_2(111)$ and $Ce_{0.96}Fe_{0.04}O_2(111)$ surfaces are plotted.

The activation Gibbs free energy (G_a) and Gibbs free energy change (ΔG) for each step in Hg oxidation can be obtained by the following eqs. (2) and (3):

$$G_a = (G_{TS} - G_R) \qquad (2)$$

$$\Delta G = (G_P - G_R) \qquad (3)$$

G_{TS}, G_R, and G_P represent Gibbs free energy of transition states, reactants, and products, respectively.

G is defined as the following formula (4)[47]:

$$G = E_{total} + E_{ZPE} + U - TS + \gamma RT \qquad (4)$$

where E_{total} is the total energy of different species in the reaction process, T is the temperature for Hg oxidation, R is gas constant, and γ is 0 for gas–solid reaction and 1 for small molecules in gas phase. E_{ZPE}, U, and S are calculated as the following equations.

E_{ZPE} refers to the zero-point vibrational energy, which is calculated by formula (5):

$$E_{ZPE} = \sum_{i=1}^{Vibrations} \frac{hv_i}{2} \qquad (5)$$

where v_i represents the vibrational frequencies of reactants, products, and transition states, and h is Planck constant.

U and S are given by the formulas (6) and (7):

$$U = RT \sum_i \left[\frac{hv_i/k_BT}{e^{hv_i/k_BT} - 1} \right] \qquad (6)$$

$$S = R \sum_i \left[\frac{hv_i/k_BT}{e^{hv_i/k_BT} - 1} - \ln\left(1 - e^{-hv_i/k_BT}\right) \right] \qquad (7)$$

where k_B is Boltzmann constant.

Results and Discussion

Analysis of Hg oxidation via the lattice O

CeO_2 exhibits impressive storage and release properties,[48,49] lattice O is very active and O vacancies on CeO_2 surface have attracted intense interest.[50] The extremely weak adsorption of Hg on the $CeO_2(111)$ surface (-4.6 kJ·mol^{-1}) implies that Hg cannot be captured effectively on the $CeO_2(111)$ surface.[28] Let us suppose Hg can be oxidized via the lattice O, HgO will be formed and adsorbed on the $CeO_{2-x}(111)$ surface. Therefore, adsorption configures of HgO on the $CeO_{2-x}(111)$ surface with adsorption energies are shown in Figure 2. We can note that V-HgO(a), (b), (c), and (d) exhibit dissociative adsorption. The dissociated O atom fills O vacancy and Hg desorbs from the surface in V-HgO(a) and (b), and the dissociated O atom adsorbed at Ce-O bridge site and Hg is away from the surface in V-HgO (c) and (d). The distances between Hg and O are 3.698, 3.706, 3.592, and 3.018 Å in these four configurations, and adsorption energies are -487.7, -486.7, -226.2, and -248.4 kJ·mol^{-1}, respectively. In V-HgO(e), HgO tilts on the surface via O and binding with surface Ce atom. An energy of -191.3 kJ·mol^{-1} is obtained for adsorption.

It can be observed that the formed HgO via lattice O oxidizing Hg cannot be existed on the surface when HgO adsorbs
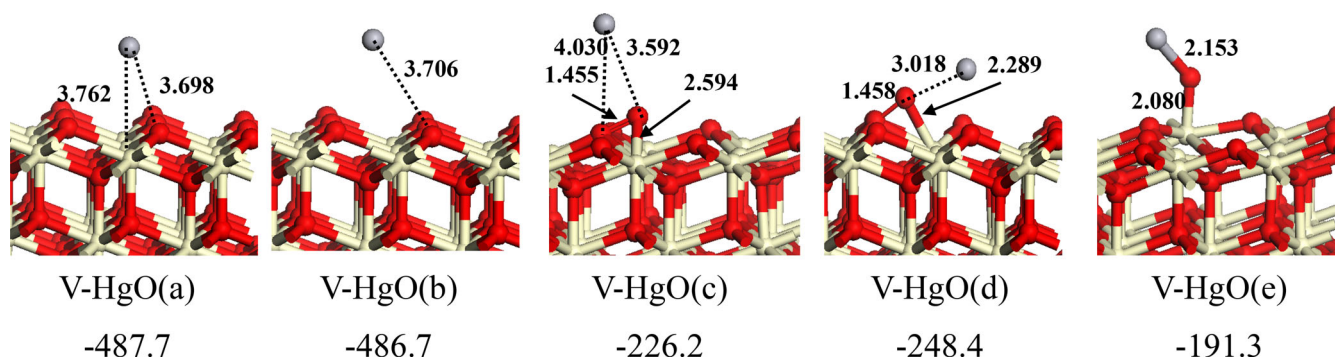

Figure 2. Optimized structures of HgO on the $CeO_{2-x}(111)$ surface with adsorption energies (kJ·mol^{-1}). [Color figure can be viewed at wileyonlinelibrary.com]

Wiley Online Library

J. Comput. Chem. **2019**, *40*, 2611–2621 **2613**

near the vacancy. O in HgO is inclined to fill the vacancy or adsorb on the surface. Meanwhile, Hg desorbs from the surface, which cannot reach the aim of removing Hg. In addition, we also see that HgO can exist on the perfect surface according to V-HgO(e) when HgO is placed away from the vacancy in the initial configuration. Therefore, we consider the effect of surface-adsorbed O on the oxidation of Hg in the following section.

Hg adsorption with different O coverage on CeO$_2$(111)

Adsorption configurations of one, two, and three O atoms on CeO$_2$(111) are constructed, the coverage of O are 0.11, 0.22, and 0.33, respectively. One O atom is adsorbed at Ce-Ce bridge and bonding with lattice O, the lengths of two O—Ce bonds are 2.498 and 2.506 Å, as shown in 1O. The most stable configurations of two and three O atoms on CeO$_2$(111) surface can be regarded as 2O and 3O in Figure 3.

When Hg is adsorbed on CeO$_2$(111) with 0.11 coverage of O, Hg is 4.500 Å distant from the surface-adsorbed O atom, stating clearly that an extremely interaction between Hg and the surface, which is proved by the little adsorption energy of −3.6 kJ·mol^{-1}. In addition, adsorption energies of Hg on CeO$_2$(111) surface with 0.22 and 0.33 coverage of O are only −3.3 and −3.2 kJ·mol^{-1}. It is demonstrated that the capture ability of Hg is not improved via adsorbing O atom on the CeO$_2$(111) surface, and the effect of different O coverage on the adsorption of Hg is negligible. In contrast, it is different from that Hg adsorption on the α-Fe$_2$O$_3$(001) surface, which changes from weak chemisorption at O coverage of 0.25 ML to stronger chemisorption at 1 ML of O coverage.[51] However, oxidation ability of surface-adsorbed O is needed to be explored in order to capture Hg. Subsequently, HgO adsorption on regular CeO$_2$(111) surface is first investigated.
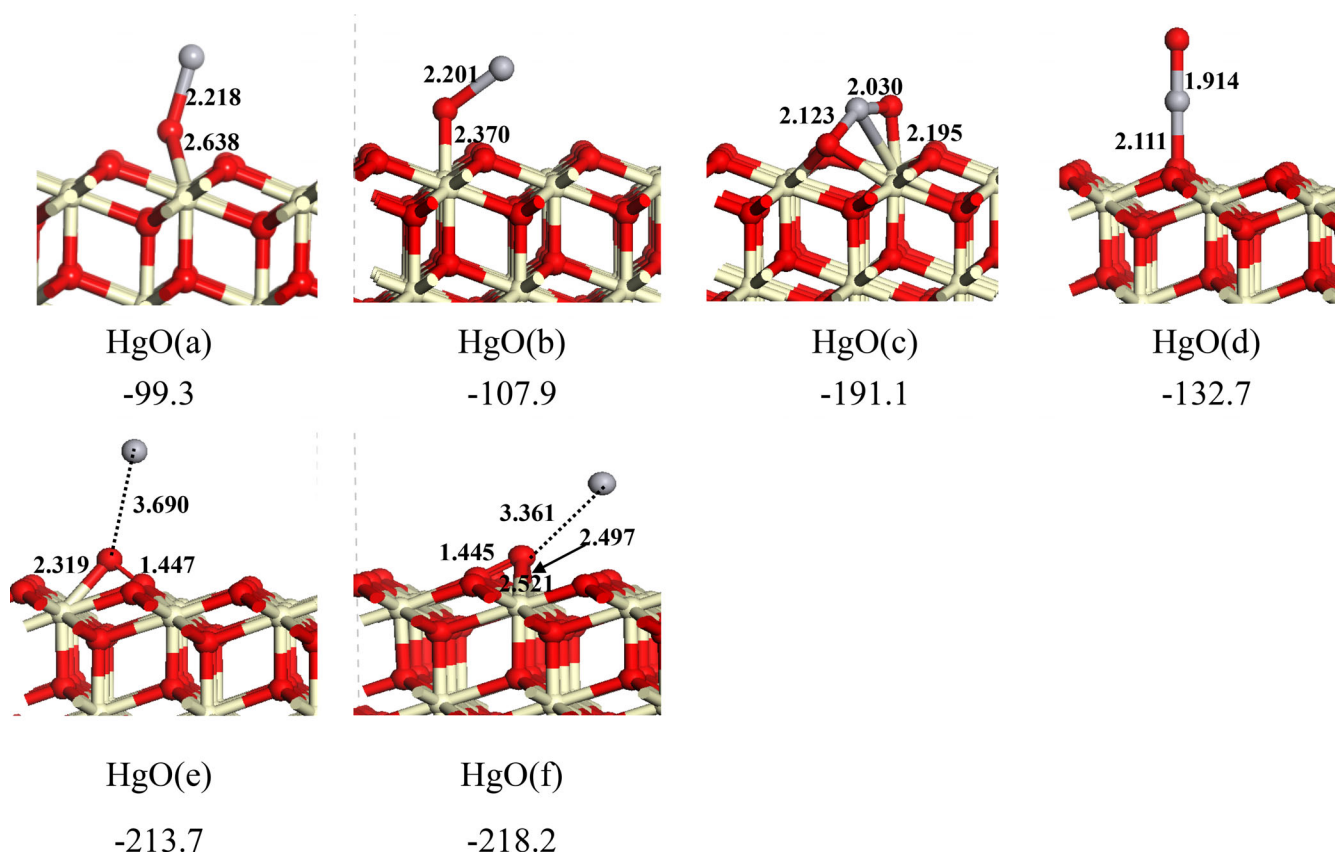
HgO adsorption on regular CeO$_2$(111) surface

HgO is with the similar structure to HgS, and the same three initial adsorption models are considered.[28] Two types of adsorption configurations for HgO, including molecular and dissociated one are also obtained, as shown in Figure 4. Four stable molecular structures of HgO on regular CeO$_2$(111) are obtained. HgO adsorbs at Ce-Ce bridge and Ce-top site via O end in HgO(a) and (b). Adsorption energies of HgO are −99.3 and −107.9 kJ·mol^{-1}, implying that they are chemisorption. HgO is parallel adsorbed on the surface in HgO(c), Hg and O in HgO bind with surface O atom and Ce via an energy of −191.1 kJ·mol^{-1}. We can see that this is a strong chemisorption. In the configuration of HgO(d), HgO is vertical adsorbed on the lattice O via Hg end, and the length between Hg and O is 2.111 Å. An energy of adsorption with −132.7 kJ·mol^{-1} also intimates that it is a relatively strong chemisorption. When O in HgO strongly adsorbs on the surface, Hg breaks away from the surface, and two dissociated configurations are obtained, as shown in HgO(e) and (f). The dissociative adsorption energies are −213.7 and −218.2 kJ·mol^{-1}, respectively. They are a little higher than that of HgO(c), which shows that HgO can exist on the surface with the molecular mode, and the parallel adsorption configuration is the most stable. It is different from the adsorption of HgS, the adsorption energy of the most stable dissociated mode is largely higher than that of the most stable molecular mode.[28] Therefore, the oxidization process of Hg to HgO via the surface-adsorbed O will be researched.

Hg oxidation via surface-adsorbed O atom

It is a negligible effect of different O coverage on the adsorption of Hg; therefore, Hg oxidation on regular CeO$_2$(111) surface with 0.11 ML coverage of O atom is investigated. The
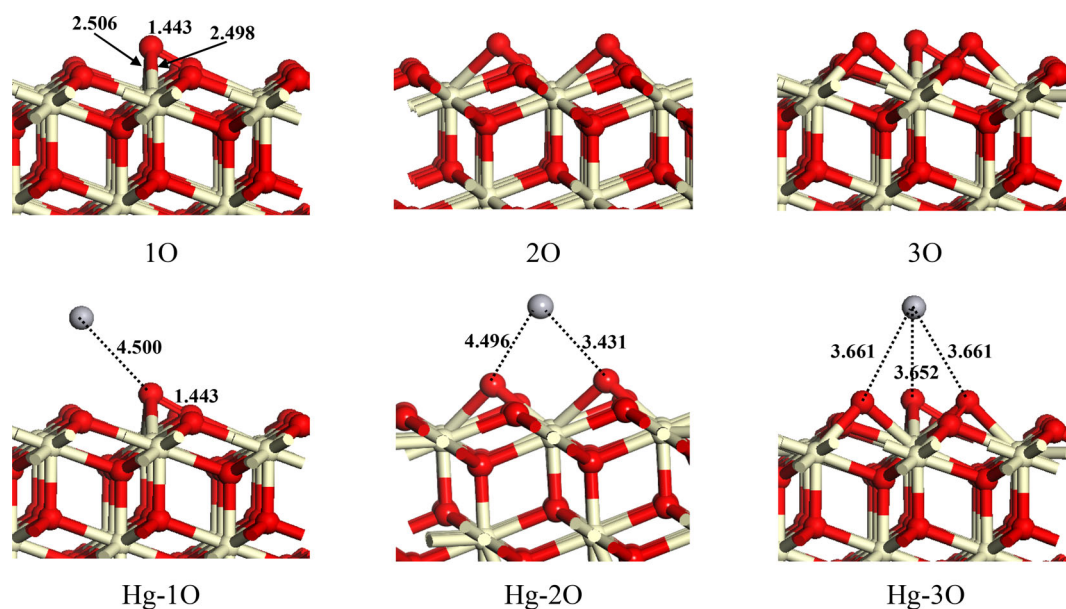
Figure 3. Stable adsorption configurations of Hg on regular CeO$_2$(111) surface with various coverage (1O, 2O, and 3O represent coverage of 0.11, 0.22 and 0.33 ML). [Color figure can be viewed at wileyonlinelibrary.com]

Figure 4. Optimized configurations of HgO on regular $CeO_2(111)$ surface with adsorption energies (kJ·mol^{-1}). [Color figure can be viewed at wileyonlinelibrary.com]

temperature range of Hg oxidation on CeO_2 is 423–623 K in the experiment,[52] and 523 K has been used to investigate the Hg oxidation in this theoretical study.

The Gibbs free energy profile of Hg oxidation to HgO including the entropy effect at 523 K on regular $CeO_2(111)$ is shown in Figure 5. Hg adsorption on $CeO_2(111)$ with one O atom (Hg-1O) is as the reactant, and the most stable molecular adsorption mode, HgO(c) is selected as the product. Hg can be oxidized to HgO by O atom which is adsorbed on the surface, this process requires a Gibbs free activation energy of 114.1 kJ·mol^{-1}. During this process, the distance between Hg

and O changes from 4.500 Å in R via 2.064 Å in TS to 2.030 Å in P, signifying that HgO is formed. In fact, we also get the conclusion that the pre-adsorbed O on $CeO_2(111)$ can be as oxidant, which is favorable for the oxidation of Hg and improve the capture efficiency of Hg.

Mn and Fe doping promote Hg capture on $CeO_2(111)$, and Hg can be easily oxidized to HgS on $Ce_{0.96}Mn_{0.04}O_2(111)$ and $Ce_{0.96}Fe_{0.04}O_2(111)$ surfaces.[28] Therefore, the effect of doped metal on the activity of lattice O, as well as on the oxidation of Hg via the lattice O will be considered.
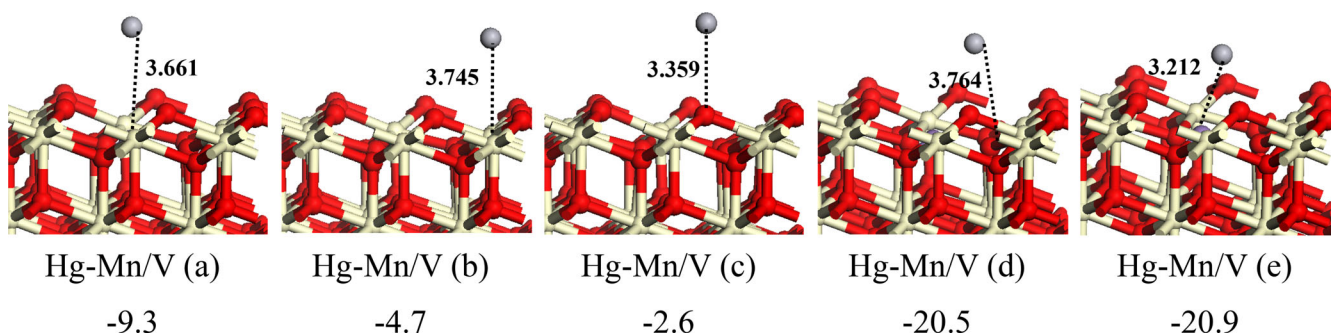
Hg adsorption on the defective $Ce_{0.96}Mn_{0.04}O_{2-x}(111)$

Mn dopant greatly promotes Hg adsorption with a significantly higher energy of −156.5 kJ·mol^{-1} than that on regular surface.[28] It is in agreement with that doping Mn greatly increases the adsorption of NO_2 on regular $CeO_2(111)$.[21] Additionally, Mn dopant can improve the activity of lattice O, and the formation energy of O vacancy is largely lower than that on regular $CeO_2(111)$.[21] Moreover, O vacancies on the surface can be seen as active sites for the reaction.[20] Thus, the adsorption of Hg on $Ce_{0.96}Mn_{0.04}O_{2-x}(111)$ surface with O vacancy will be investigated.

Hg adsorbs at Ce-top site in Hg-Mn/V (a) and (b) with different Ce atoms on $Ce_{0.96}Mn_{0.04}O_{2-x}(111)$ (Fig. 6). The distances between Hg and Ce are 3.661 and 3.745 Å, and very low adsorption energies of −9.3 and − 4.7 kJ·mol^{-1} are obtained,
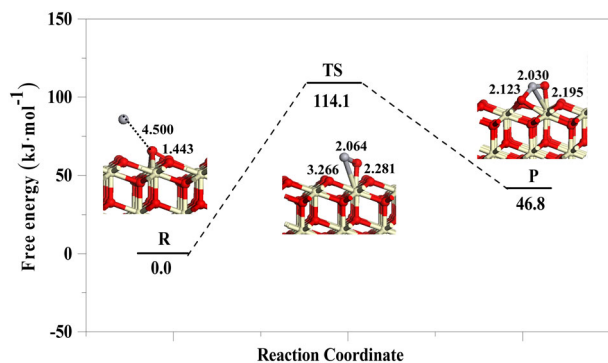
Figure 5. Gibbs free energy profile of Hg oxidation by surface-adsorbed O at 523 K on regular $CeO_2(111)$ surface. [Color figure can be viewed at wileyonlinelibrary.com]

Figure 6. Optimized configurations of Hg on the defective $Ce_{0.96}Mn_{0.04}O_{2-x}$(111) surface with adsorption energies (kJ·mol^{-1}). [Color figure can be viewed at wileyonlinelibrary.com]

respectively. For Hg-Mn/V (c) and (d), Hg adsorbs at O1-top and O_{sub} sites, the distances between Hg and O are 3.359 and 3.764 Å with energies of −2.6 and − 20.5 kJ·mol^{-1} for Hg adsorption, respectively. Hg adsorbs at the top site of doped Mn, the adsorption energy of Hg is −20.9 kJ·mol^{-1}, as shown in Hg-Mn/V (e). It is the most stable configuration for Hg adsorption on the defective $Ce_{0.96}Mn_{0.04}O_{2-x}$(111) surface, which is owned to physical adsorption and is far weaker than that on the $Ce_{0.96}Mn_{0.04}O_2$(111) surface.

It is not hard to find that the lattice O atom has a strong interaction with Hg and is enough to oxidize Hg to HgO when Mn atom is doped on regular CeO_2(111). Moreover, the adsorption ability of defective $Ce_{0.96}Mn_{0.04}O_{2-x}$(111) surface to Hg is very weak, thus the $Ce_{0.96}Mn_{0.04}O_{2-x}$(111) surface is difficult to further oxidize Hg through lattice O atom, and the oxidation of Hg by the lattice O atom on $Ce_{0.96}Mn_{0.04}O_{2-x}$(111) surface will not be considered. When defective $Ce_{0.96}Mn_{0.04}O_{2-x}$(111) surface is reduced by oxygen, it will form an O-containing surface, which will continue to oxidize Hg to HgO. Meanwhile, the generated HgO adsorbs on the $Ce_{0.96}Mn_{0.04}O_2$(111) surface; therefore, adsorption of HgO on defective $Ce_{0.96}Mn_{0.04}O_{2-x}$(111) and $Ce_{0.96}Mn_{0.04}O_2$(111) surfaces will be explored in the next section.

Adsorption of HgO on $Ce_{0.96}Mn_{0.04}O_{2-x}$(111) and $Ce_{0.96}Mn_{0.04}O_2$(111) surfaces

The adsorption of HgO on the $Ce_{0.96}Mn_{0.04}O_{2-x}$(111) surface is first investigated, and stable adsorption configurations with adsorption energies are shown in Figure 7. HgO is dissociated in HgO-Mn/V (a) and (b), and the dissociated O atom fills the surface O vacancy and O adsorbed at Ce-Ce bridge site binding with O1, respectively. The lengths of Hg—O bonds are stretched to 3.368 and 4.293 Å comparing with 2.100 Å in gas phase. The dissociative adsorption energies are −332.8 and −264.3 kJ·mol^{-1}. When HgO is vertical placed at O_v site by Hg end and O end, the HgO can be stable in molecular form at O_v site, and adsorption energies are −38.1 and −256.0 kJ·mol^{-1}, as shown in HgO-Mn/V (c) and (d). In HgO-Mn/V (d), HgO strongly adsorbs at the O_v site and O atom binds with the doped Mn atom. For HgO-Mn/V (e), the surface O vacancy is filled with the O atom of HgO, and Hg binds with O1 and Mn. It can be seen that the configuration is highly similar to Hg adsorption on the
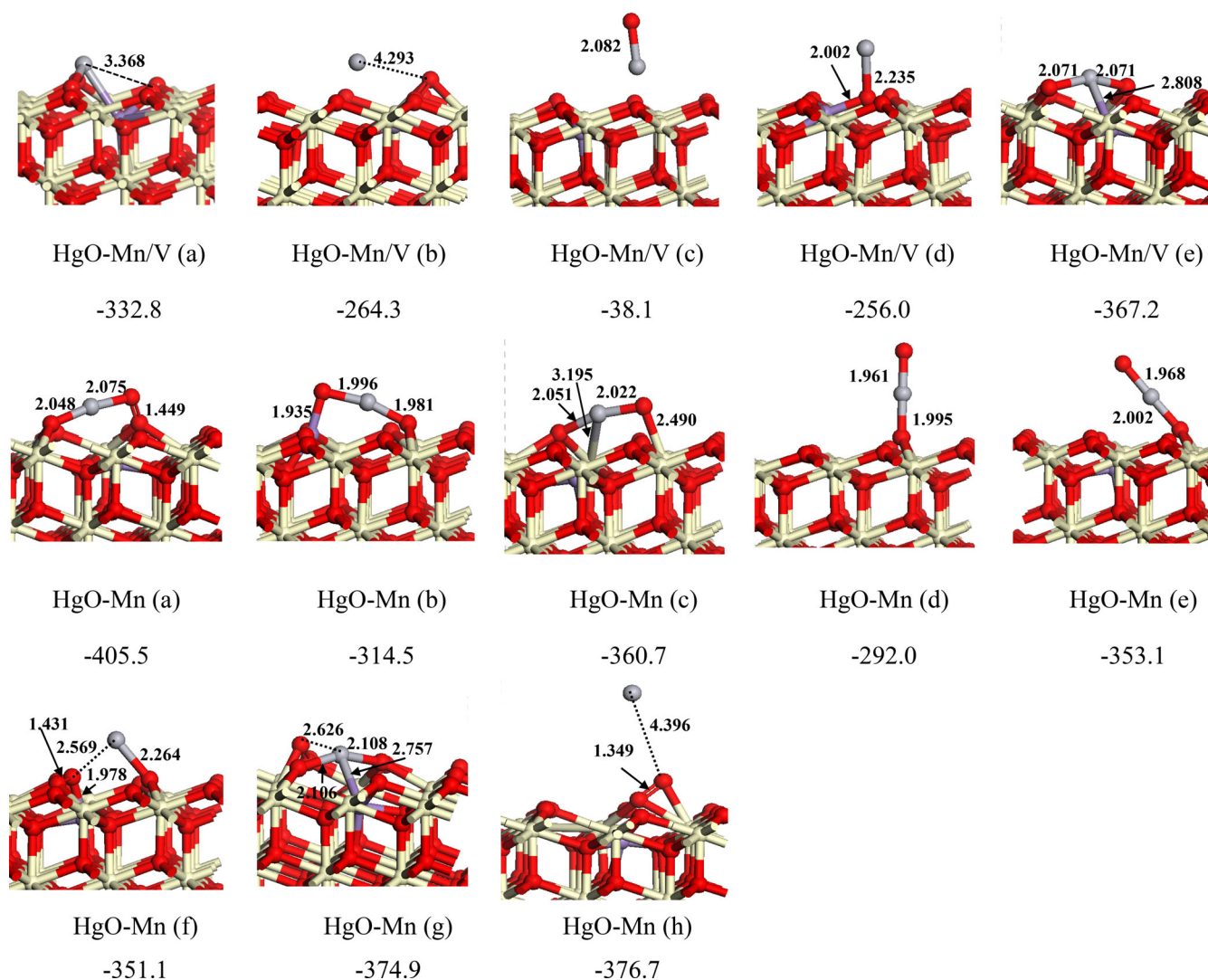
$Ce_{0.96}Mn_{0.04}O_2$(111) surface, and the adsorption energy is the highest with −367.2 kJ·mol^{-1}. It is therefore clear that HgO prefers to exist in molecular form on the $Ce_{0.96}Mn_{0.04}O_{2-x}$(111) surface, and the lattice O atom on $Ce_{0.96}Mn_{0.04}O_2$(111) surface can oxidize Hg to HgO.

HgO tilts on the $Ce_{0.96}Mn_{0.04}O_2$(111) surface in molecular mode in HgO-Mn (a), (b), and (c) with different interaction sites. HgO adsorbs at O1-O1 bridge site, binds with O1 and Mn, as well as O1 and Ce at three configurations with great adsorption energies of −405.5, −314.5 and −360.7 kJ·mol^{-1}. In HgO-Mn (d) and (e), HgO is adsorbed on the surface by Hg end, the lengths of Hg-O1 bonds are 1.995 and 2.002 Å, two relative high energies of −292.0 and −353.1 kJ·mol^{-1} are got. Moreover, three dissociated adsorption configurations are generated. The dissociated Hg is adsorbed at O1 site, and Hg-O bond is elongated to 2.569 Å in HgO-Mn (f). While the dissociated Hg bind with Mn, as well as two surfaces O1 in HgO-Mn (g). The adsorption energies of these two configurations are −351.1 and −374.9 kJ·mol^{-1}, respectively. In HgO-Mn (h), the dissociated O is adsorbed at Ce-O1 bridge site, and Hg desorbs from the surface with 4.396 Å between Hg and O, the dissociative adsorption energy is −376.7 kJ·mol^{-1}. We can observe that HgO mainly adsorbs on $Ce_{0.96}Mn_{0.04}O_2$(111) in molecular form and HgO-Mn (a) is the most stable.

Cyclic oxidation of Hg on the $Ce_{0.96}Mn_{0.04}O_2$(111) surface

A catalytic cycle for Hg oxidation at 523 K on the $Ce_{0.96}Mn_{0.04}O_2$(111) surface followed by the Mars-van Krevelen mechanism is obtained, as shown in Figure 8. A similar study of the oxidation of CO on the Ru-doped CeO_2(111) surface has been done in previous work.[53] The cyclic oxidation mainly consists of three processes. The whole process begins with the first oxidation of Hg.

When Hg is adsorbed on the $Ce_{0.96}Mn_{0.04}O_2$(111) surface, the lattice O directly oxidizes Hg to HgO without any activation barrier. The former structure is equivalent to HgO on the $Ce_{0.96}Mn_{0.04}O_{2-x}$(111) surface, and the most stable structure HgO-Mn/V(e) is selected. And then $Ce_{0.96}Mn_{0.04}O_{2-x}$(111) surface is established with the desorption of HgO molecule. It coincides well with the study of Hsu et al.,[18] the lattice O was activated in a great degree when CeO_2(111) surface was doped with metal Mn, which led to the production of surface O vacancy

Figure 7. Optimized configurations of HgO on $Ce_{0.96}Mn_{0.04}O_{2-x}(111)$ and $Ce_{0.96}Mn_{0.04}O_2(111)$ surfaces with adsorption energies (kJ·mol^{-1}). [Color figure can be viewed at wileyonlinelibrary.com]

easily. This is an essential prerequisite for this cyclic process to be completed. The second process is the regeneration of the $Ce_{0.96}Mn_{0.04}O_2(111)$ surface in an oxygen atmosphere. O_2 molecule adsorbs at the O vacancy position and a $Ce_{0.96}Mn_{0.04}O_2(111)$ surface with a adsorption of O atom is formed, as shown in LM1. It is indicated that the reduced surface can be filled by O_2 molecule from the gas phase. The adsorbed O on the surface should be active according to the oxidation of Hg on the $CeO_2(111)$ surface with a adsorbed O atom. And the last process of cyclic oxidation is the second oxidation of Hg by the O adspecies, following by the second regeneration of the $Ce_{0.96}Mn_{0.04}O_2(111)$ surface. A Gibbs free energy of 1.4 kJ·mol^{-1} changes for the second Hg adsorption on the $Ce_{0.96}Mn_{0.04}O_2(111)$ surface with an adsorbed O atom, implying the adsorption of Hg is very weak, as shown in LM2. Similarly, the surface-adsorbed O oxidizes Hg to generate the second HgO, which needs to overcome a Gibbs activation energy barrier of 70.7 kJ·mol^{-1} with a change of Gibbs free energy of −17.2 kJ·mol^{-1} for this oxidation reaction. Hg—O

bond of 4.599 Å in LM2 via 3.017 Å in MnCe-TS1 is shortened to 2.075 Å in HgO-Mn(a). HgO desorbs from the surface and a perfect $Ce_{0.96}Mn_{0.04}O_2(111)$ surface is generated. The whole oxidation process of Hg on the $Ce_{0.96}Mn_{0.04}O_2(111)$ surface is stopped here and this process will repeat over and over again. This cyclic oxidation process has been found for the oxidation of CO on Mn-, Ru-, Pt-, and Au-doped $CeO_2(111)$ surfaces,[18,20,53,54] implying the lattice O on ceria surface is with extreme activity. Additionally, Mn doped in CeO_2-ZrO_2 catalyst increased the quantity of surface-adsorbed O and exhibited an outstanding Hg oxidation efficiency, therefore enhanced the redox properties.[55]

In order to further understand the cyclic process of Hg oxidation on the $Ce_{0.96}Mn_{0.04}O_2(111)$ surface, the Bader charge of the doped Mn atom in different structures involved in this cyclic process are calculated, which are shown in Table 1. Bader charges of Mn^{2+} and Mn^{4+} in pure MnO and MnO_2 are 5.67 and 5.35 e, respectively. The valence states of Mn in different species are deduced according to the calculated Bader charge. In
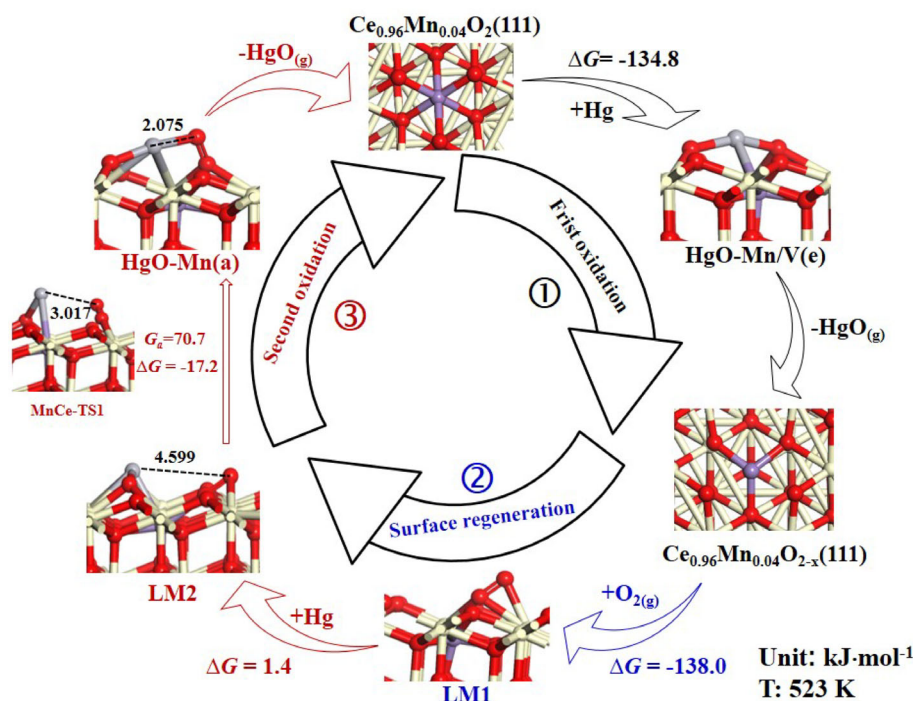
Wiley Online Library

J. Comput. Chem. **2019**, *40*, 2611–2621 **2617**

Figure 8. Gibbs free energy profile of Hg cyclic oxidation at 523 K on the $Ce_{0.96}Mn_{0.04}O_2(111)$ surface. [Color figure can be viewed at wileyonlinelibrary.com]

$Ce_{0.96}Mn_{0.04}O_2(111)$, Mn^{4+} is doped in the perfect $CeO_2(111)$ surface via substituting one Ce atom, which is in good agreement with the result of Hsu et al.[18] And then Mn^{4+} is reduced to Mn^{2+} as HgO forming and absorbing on the defective surface. The formation of $Ce_{0.96}Mn_{0.04}O_{2-x}(111)$ results in the oxidation state of Mn is between Mn^{2+} and Mn^{4+}, which is denoted as $Mn^{\delta+}$. When O_2 molecule adsorbs on the defective surface, the $Ce_{0.96}Mn_{0.04}O_2(111)$ surface is regenerated, and the valence state of Mn is also changed to 4+. However, an oxidation state of 2+ for Mn is formed because Hg stably adsorbs on the surface binding with Mn, Ce, and O atom. The valence state of Mn changes from Mn^{2+} to $Mn^{\delta+}$ along with the Hg oxidation on the surface. Finally, Mn is in the oxidation state of 4+ on the $Ce_{0.96}Mn_{0.04}O_2(111)$ surface followed by the end of cyclic oxidation process.

Hg removal on the $Ce_{0.96}Fe_{0.04}O_2(111)$ surface

CeO_2 doping Fe catalyst has been prepared[56] and acquired good catalytic result in industry,[57,58] Moreover, CO can be cyclic oxidized on the Fe-doped $CeO_2(111)$ surface through the

DFT + U method. Fe dopant favored the O vacancy formation and facilitated the CO oxidation.[59] Therefore, the effect of $Ce_{0.96}Fe_{0.04}O_2(111)$ surface on the oxidation of Hg is investigated in this work.

Analogous to the study of Hg removal on the $Ce_{0.96}Mn_{0.04}O_2(111)$ surface, adsorption of Hg on $Ce_{0.96}Fe_{0.04}O_{2-x}(111)$, HgO on $Ce_{0.96}Fe_{0.04}O_{2-x}(111)$, and $Ce_{0.96}Fe_{0.04}O_2(111)$ surfaces are studied (Supporting Information Fig. S1 and S2).

The oxidation reaction mechanism of Hg at 523 K on the $Ce_{0.96}Fe_{0.04}O_2(111)$ surface is similar to the Mn-doped surface, and the whole mechanism also contains three processes, as shown in Figure 9. Hg atom is adsorbed on the surface forming the configuration of Hg-Fe, and Hg will be oxidized to HgO by lattice O. This process needs to overcome a small Gibbs free energy barrier of 12.3 $kJ \cdot mol^{-1}$, and Gibbs free energy of -35.1 $kJ \cdot mol^{-1}$ changes for this oxidation. The distance between Hg and O from 2.478 Å in Hg-Fe shortens to 2.069 Å in HgO-Fe/V(c) via 2.370 Å in FeCe-TS1. In this process, the oxidation state of doped Fe atom is Fe^{3+}, implying that Fe^{3+} is favorable for the Hg oxidation. Similarly, incorporated Fe^{3+} led to the formation of CO_2 during CO oxidation on the $Ce_{0.875}Fe_{0.125}O_2(111)$ surface.[59] Subsequently, HgO molecule leaves the $Ce_{0.96}Fe_{0.04}O_2(111)$ surface leading to the formation of O vacancy surface. The Bader charge of Fe neighboring the O vacancy is 6.40 e, implying that Fe is still in the 3+ oxidation state, which is coincident with Chen' result.[59] This is the first oxidation of Hg. The second stage is the regeneration of surface, in which the $Ce_{0.96}Fe_{0.04}O_2(111)$ surface will be generated via one O atom filling the vacancy on the defective $Ce_{0.96}Fe_{0.04}O_{2-x}(111)$ surface, and the other O atom of oxygen molecule adsorbs on the $Ce_{0.96}Fe_{0.04}O_2(111)$ surface (LM1). The third stage is the second oxidation of Hg, the adsorbed Hg will be oxidized by the co-adsorbed O atom on the $Ce_{0.96}Fe_{0.04}O_2(111)$ surface leading to the formation of HgO. An activation Gibbs free energy of 49.6 $kJ \cdot mol^{-1}$ is needed

Table 1. Calculated Bader charge of Mn atoms in the oxidation cyclic process.

Oxidation cyclic process	Structures	Bader charge of Mn (e)	Valence state of Mn
Frist oxidation	$Ce_{0.96}Mn_{0.04}O_2(111)$	5.37	Mn^{4+}
	HgO-Mn/V(e)	5.60	Mn^{2+}
Surface regeneration	$Ce_{0.96}Mn_{0.04}O_{2-x}(111)$	5.50	$Mn^{\delta+}$
	LM1	5.39	Mn^{4+}
Second oxidation	LM2	5.65	Mn^{2+}
	MnCe-TS1	5.57	$Mn^{\delta+}$
	HgO-Mn(a)	5.57	$Mn^{\delta+}$
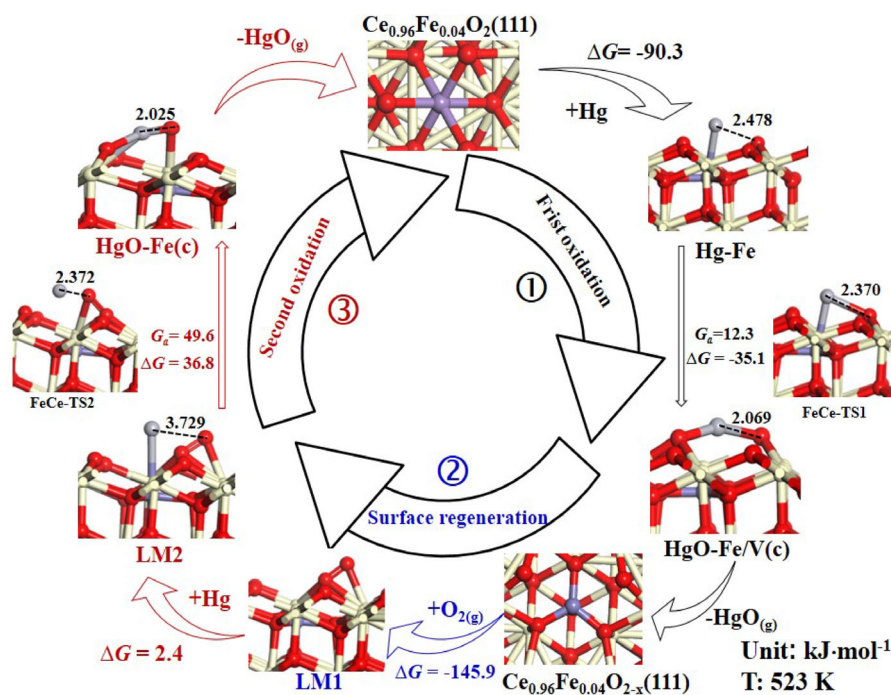
Figure 9. Gibbs free energy profile of Hg cyclic oxidation at 523 K on the $Ce_{0.96}Fe_{0.04}O_2(111)$ surface. [Color figure can be viewed at wileyonlinelibrary.com]

in this process at FeCe-TS2, and the distance between Hg and O from 3.729 Å (LM2) shortens to 2.025 Å [HgO-Fe(c)]. The Gibbs free energy change is 36.8 kJ·mol^{-1} for this oxidation. Eventually, HgO leaves the surface and leads to the formation of a perfect $Ce_{0.96}Fe_{0.04}O_2(111)$ surface. During the process of Hg removal by Cu-Ce mixed oxides, adsorbed Hg was oxidized, and CeO_2 also played a role of redox cycle, which projected an excellent stability and reusability for Hg removal.[60] By analyzing the Bader charge in Table 2, it is not difficult to find that the main oxidation state of Fe in the whole process is Fe^{3+}. We can be sure that Fe^{3+} contributes to the establishment of the cyclic oxidation process of Hg, which is good consistent with the results obtained by Chen et al.[59]

The role of surface O in removing Hg

Two types of O on the regular $CeO_2(111)$ surface, including surface-adsorbed O and lattice O, play an important role for the removal of Hg. The surface-adsorbed O can oxidize Hg to HgO at 523 K with Gibbs activaiton energies of 114.1, 70.7, and

49.6 kJ·mol^{-1} on un-doped, Mn- and Fe-doped $CeO_2(111)$ surface, respectively. It implies that Hg can be captured in the form of HgO via the oxidation by surface-adsorbed O, which can effectively promote Hg removal. And Mn and Fe dopant get a promotional effect on the oxidation of Hg via the adsorbed O on the surface.

In addition, the role of lattice O is not negligible for Hg oxidation. Lattice O on the un-doped $CeO_2(111)$ is inert to Hg oxidation, but Mn and Fe dopant increase the activity of lattice of $CeO_2(111)$. Hg can be oxidized directly to HgO by surface lattice O without an energy barrier on the $Ce_{0.96}Mn_{0.04}O_2(111)$ surface, which is consistent that Mn dopant decreases the O-vacancy formation energy,[61] and promotes CO oxidaiton without any activaiton energy.[18] For the Fe-doped surface, Hg can still be oxidized to HgO by lattice O with a very low activation Gibbs free energy of 12.3 kJ·mol^{-1}. Although the activity of lattice O on Fe-doped surface is less than that of Mn-doped surface due to higher O-vacancy formation energy of the Fe-doped ceria,[18,61] Fe still greatly improves the oxidation ability of lattice O on $CeO_2(111)$ surface, which is similar to the oxidation of CO on $Ce_{0.96}Fe_{0.04}O_2(111)$ surface, and the oxidation product CO_2 is observed.[62] The second oxidaiton of Hg via the adsorbed O on the surface shows that Hg is little harder to be oxidized on the $Ce_{0.96}Mn_{0.04}O_2(111)$ surface with an activation Gibbs free energy of 70.7 kJ·mol^{-1} than that on the $Ce_{0.96}Fe_{0.04}O_2(111)$ surface with 49.6 kJ·mol^{-1}. However, Mn-terminated $MnFe_2O_4(100)$ surface is much more favorable for Hg oxidation by surface-adsorbed O than Fe-terminated surface, and energy barriers of Hg oxidation are 76.1 kJ·mol^{-1} on Mn-terminated surface and 206.4 kJ·mol^{-1} on Fe-terminated surface, respectively.[63]

Conclusions

The removal mechanisms of Hg on un-doped, Mn-, and Fe-doped $CeO_2(111)$ have been investigated in this study. The

Table 2. Calculated Bader charge of Fe atoms in the oxidation cyclic process.[a]

Oxidation cyclic process	Structures	Bader charge of Fe (e)	Valence state of Fe
Frist oxidation	$Ce_{0.96}Fe_{0.04}O_2(111)$	6.43	Fe^{3+}
	Hg-Fe	6.40	Fe^{3+}
	FeCe-TS1	6.41	Fe^{3+}
	HgO-Fe/V(c)	6.49	Fe^{3+}
Surface regeneration	$Ce_{0.96}Fe_{0.04}O_{2-x}(111)$	6.40	Fe^{3+}
	LM1	6.44	Fe^{3+}
Second oxidation	LM2	6.39	Fe^{3+}
	FeCe-TS2	6.48	Fe^{3+}
	HgO-Fe(c)	6.38	Fe^{3+}

[a] Calculated Bader charges of Fe in FeO and Fe_2O_3 are 6.73 and 6.53 e, respectively.

adsorption of Hg on the un-doped $CeO_2(111)$ surface and HgO on $CeO_{2-x}(111)$ surface are first studied. The result demonstrates that the activity of lattice O on the un-doped $CeO_2(111)$ surface is insufficient to oxidize Hg to HgO. While Hg can be oxidized to HgO via the adsorbed O on the regular $CeO_2(111)$ surface with an activation Gibbs free energy of 114.1 kJ·mol^{-1}. Additionally, coverage of O has insignificant effect on the adsorption of Hg.

Moreover, the second metals (Mn and Fe) are introduced into $CeO_2(111)$, which greatly improves the adsorption ability of $CeO_2(111)$ surface to Hg, the adsorption energies of Hg are −156.5 and −97.2 kJ·mol^{-1}, largely higher than that of −4.6 kJ·mol^{-1} on the un-doped surface. The activity of the lattice O on the regular $CeO_2(111)$ is also promoted, Hg is oxidized to HgO without a activation energy on $Ce_{0.96}Mn_{0.04}O_2(111)$ and a little activation Gibbs free energy of 12.3 kJ·mol^{-1} is needed on $Ce_{0.96}Fe_{0.04}O_2(111)$. In addition, the dopants of Mn and Fe reduce the Gibbs free energy of activation for Hg oxidation by surface-adsorbed O. It needs to overcome Gibbs free energy barriers of 70.7 and 49.6 kJ·mol^{-1} on $Ce_{0.96}Mn_{0.04}O_2(111)$ and $Ce_{0.96}Fe_{0.04}O_2(111)$ surfaces, which are lower than that on the un-doped surface. Therefore, the pre-oxidation of the ceria catalyst is beneficial to the removal of Hg.

Acknowledgments

[1] C. B. Gopal, M. G. Melchor, S. C. Lee, Y. Z. Shi, A. Shavorskiy, M. Monti, Z. X. Guan, R. Sinclair, H. Bluhm, A. Vojvodic, W. C. Chueh, *Nat. Commun.* **2017**, *8*, 15360.
[2] Y. Yang, J. Liu, Z. Wang, F. Liu, *Dent. Tech.* **2018**, *174*, 17.
[3] Y. Su, J. Liu, I. A. W. Filot, L. Zhang, E. J. M. Hensen, *ACS Catal.* **2018**, *8*, 6552.
[4] R. Yang, Y. Liu, L. Yu, X. Zhao, X. Yang, M. Sun, J. Luo, Q. Fan, J. Xiao, Y. Zhao, *J. Nanopart. Res.* **2018**, *20*, 138.
[5] S. Zhao, Y. Duan, T. Yao, M. Liu, J. Lu, H. Tan, X. Wang, *Fuel* **2017**, *199*, 653.
[6] C. Chun, Y. Cao, S. Liu, J. Chen, W. Jia, *Fuel Process. Dent. Tech.* **2018**, *181*, 268.
[7] K. H. Liu, M. Y. Chen, Y. C. Tsai, H. P. Lin, H. C. His, *Catal. Today* **2017**, *279*, 104.
[8] L. Ling, M. Fan, B. Wang, R. Zhang, *Energy Environ. Sci.* **2015**, *8*, 3109.
[9] C. T. Driscoll, R. P. Mason, H. M. Chan, D. J. Jacob, N. Pirrone, *Environ. Sci. Technol.* **2013**, *47*, 4967.
[10] Y. M. Panta, J. Liu, M. A. Cheney, S. W. Joo, S. J. Qian, *J. Colloids Interface Sci.* **2009**, *333*, 485.
[11] D. Mergler, H. A. Anderson, L. H. M. Chan, K. R. Mahaffey, M. Murray, M. Sakamoto, A. H. Stern, *Hum. Environ* **2007**, *36*, 3.
[12] F. Wang, B. Shen, L. Gao, J. Yang, *Fuel Process. Dent. Tech.* **2017**, *168*, 131.
[13] X. P. Fan, C. T. Li, G. M. Zeng, X. Zhang, S. S. Tao, P. Lu, Y. Tan, D. Q. Luo, *Energy Fuel* **2012**, *26*, 2082.
[14] X. P. Fan, C. T. Li, G. M. Zeng, Z. Gao, L. Chen, W. Zhang, H. L. Gao, *Energy Fuel* **2010**, *24*, 4250.
[15] X. Y. Hua, J. S. Zhou, Q. K. Li, Z. Y. Luo, K. F. Cen, *Energy Fuel* **2010**, *24*, 5426.
[16] L. H. Tian, C. T. Li, Q. Li, G. M. Zeng, Z. Gao, S. H. Li, X. P. Fan, *Fuel* **2009**, *88*, 1687.
[17] H. Li, S. W. Wu, C.-Y. Wu, J. Wang, L. Li, K. Shih, *Environ. Sci. Dent. Tech.* **2015**, *49*, 7373.
[18] L. C. Hsu, M. K. Tsai, Y. H. Lu, H. T. Chen, *J. Phys. Chem. C* **2013**, *117*, 433.
[19] W. L. Cen, Y. Liu, Z. B. Wu, H. Q. Wang, X. L. Weng, *Phys. Chem. Chem. Phys.* **2012**, *14*, 5769.
[20] L. Nie, D. Mei, H. Xiong, B. Peng, Z. Ren, X. I. P. Hernandez, A. DeLaRiva, M. Wang, M. H. Enɡelhard, L. Kovarik, A. K. Datye, Y. Wang, *Science* **2017**, *358*, 1419.
[21] Y. H. Lu, H. T. Chen, *J. Phys. Chem. C* **2014**, *118*, 10043.
[22] Y. Liu, W. L. Cen, Z. B. Wu, X. L. Weng, H. Q. Wang, *J. Phys. Chem. C* **2012**, *116*, 22930.
[23] P. Wang, S. Su, J. Xiang, H. You, G. Cao, L. Sun, S. Hu, Y. Zhang, *Chemosphere* **2014**, *101*, 49.
[24] M. Nolan, S. C. Parker, G. W. Watson, *Surf. Sci.* **2005**, *595*, 223.
[25] N. V. Skorodumova, M. Baudin, K. Hermansson, *Phys. Rev. B* **2004**, *69*, 075401.
[26] X. D. Feng, D. C. Sayle, Z. L. Wang, M. S. Paras, B. Santora, A. C. Sutorik, T. X. T. Sayle, Y. Yang, Y. Ding, X. D. Wang, Y. S. Her, *Science* **2006**, *312*, 1504.
[27] D. H. Mei, N. A. Deskins, M. Dupuis, Q. F. Ge, *J. Phys. Chem. C* **2007**, *111*, 10514.
[28] L. Ling, Z. Zhao, S. Zhao, Q. Wang, B. Wang, R. Zhang, D. Li, *Appl. Surf. Sci.* **2017**, *403*, 500.
[29] B. Hammer, *Phys. Rev. B* **1999**, *59*, 7413.
[30] J. Hafner, *Comput. Phys. Commun.* **2007**, *177*, 6.
[31] J. Hafner, *J. Comput. Chem.* **2008**, *29*, 2044.
[32] P. E. Blöchl, *Phys. Rev. B* **1994**, *50*, 17953.
[33] G. Kresse, J. Furthmüller, *Comput. Mater. Sci.* **1996**, *6*, 15.
[34] S. Serrano-Zabaleta, M. A. Laguna-Bercero, L. Ortega-San-Martín, A. Larrea, *J. Eur. Ceram. Soc.* **2014**, *34*, 2123.
[35] M. M. Branda, R. M. Ferullo, M. Causà, F. Illas, *J. Phys, Chem. C* **2011**, *115*, 3716.
[36] W. Wang, S. Thevuthasan, W. Wang, P. Yang, *J. Phys. Chem. C* **2016**, *120*, 2655.
[37] Y. Choi, M. Scott, T. Söhnel, H. Idriss, *Phys. Chem. Chem. Phys.* **2014**, *16*, 22588.
[38] J. Zhang, X. Gong, G. Lu, *Chinese J. Catal.* **2014**, *35*, 1305.
[39] O. D'Alessandro, D. G. Pintos, A. Juan, B. Irigoyen, J. Sambeth, *Appl. Surf. Sci.* **2015**, *359*, 14.
[40] M. D. Krcha, M. J. Janik, *Langmuir* **2013**, *29*, 10120.
[41] S. Huang, B. E. Wilson, W. H. Smyrl, D. G. Truhlar, A. Stein, *Chem. Mater.* **2016**, *28*, 746.
[42] H.-C. Wu, O. N. Mryasov, M. Abid, K. Radican, I. V. Shvets, *Sci. Rep.* **2013**, *3*, 1830.
[43] D. Sheppard, P. Xiao, W. Chemelewski, D. D. Johnson, G. Henkelman, *J. Chem. Phys.* **2012**, *136*, 074103.
[44] D. Sheppard, G. Henkelman, *J. Chem. Phys.* **2010**, *32*, 1769.
[45] A. Heyden, A. T. Bell, F. J. Keil, *J. Chem. Phys.* **2005**, *123*, 224101.
[46] J. Kästner, P. Sherwood, *J. Chem. Phys.* **2008**, *128*, 014106.
[47] X. M. Cao, R. Burch, C. Hardacre, P. Hu, *Catal. Today* **2011**, *165*, 71.
[48] A. Trovarelli, *Comments Inorg. Chem* **1999**, *20*, 263.
[49] J. Zhang, H. Kumagai, K. Yamamura, S. Ohara, S. Takami, A. Morikawa, H. Shinjoh, K. Kaneko, T. Adschiri, A. Suda, *Nano Lett.* **2011**, *11*, 361.
[50] H. Y. Li, H. F. Wang, X. Q. Gong, Y. L. Guo, Y. Guo, G. Z. Lu, P. Hu, *Phys. Rev. B* **2009**, *79*, 193401.

[51] T. Liu, X. Guo, C. Zheng, *Fuel* **2014**, *115*, 179.

[52] X. Y. Wen, C. T. Li, X. P. Fan, H. L. Gao, W. Zhang, L. Cheng, G. G. Zhang, Y. P. Zhao, *Energy Fuel.* **2011**, *25*, 2939.

[53] H. T. Chen, *J. Phys. Chem. C* **2012**, *116*, 6239.

[54] H. Y. Kim, G. Henkelman, *J. Phys. Chem. Lett.* **2013**, *4*, 216.

[55] Z. Zhou, X. Liu, Z. Liao, H. Shao, C. Lv, Y. Hu, M. Xu, *Fuel Process. Dent. Tech.* **2016**, *152*, 285.

[56] M. S. Hegde, P. Bera, *Catal. Today.* **2015**, *253*, 40.

[57] Y. Wang, F. Wang, Y. Chen, D. Zhang, B. Li, S. Kang, X. Li, L. Cui, *Appl. Catal. Environ.* **2014**, *147*, 602.

[58] K. Li, M. Haneda, M. Ozawa, *J. Mater. Sci.* **2013**, *48*, 5733.

[59] H. T. Chen, J. G. Chang, *J. Phys. Chem. C* **2011**, *115*, 14745.

[60] W. Xu, Y. G. Adewuyi, Y. Liu, Y. Wang, *Fuel Process. Dent. Tech.* **2018**, *170*, 21.

[61] Y. Tang, H. Zhang, L. Cui, C. Ouyang, S. Shi, W. Tang, H. Li, J.-S. Lee, L. Chen, *Phys. Rev. B* **2010**, *82*, 125104.

[62] X. Liu, X. Wang, M. Yao, W. Cui, H. Yan, *Catal. Commun.* **2015**, *63*, 35.

[63] Y. Yang, J. Liu, B. Zhang, F. Liu, *J. Hazard. Mater.* **2017**, *321*, 154.

Wiley Online Library

J. Comput. Chem. **2019**, *40*, 2611–2621   **2621**